Acousto-optic deflectors in experimental neuroscience: overview of theory and applications

TOPICAL REVIEW • OPEN ACCESS

Acousto-optic deflectors in experimental neuroscience: overview of theory and applications

Journal of Physics: Photonics

OPEN ACCESS

RECEIVED
7 July 2023

REVISED
11 December 2023

ACCEPTED FOR PUBLICATION
27 February 2024

PUBLISHED
11 March 2024

TOPICAL REVIEW

Acousto-optic deflectors in experimental neuroscience: overview of theory and applications

Pietro Ricci[1,*], **Giuseppe Sancataldo**[2,*], **Vladislav Gavryusev**[3,4,5], **Francesco Saverio Pavone**[3,4,5], **Peter Saggau**[6] and **Martí Duocastella**[1,7]

[1] Department of Applied Physics, Universitat de Barcelona, Barcelona, Spain
[2] Department of Physics and Chemistry, University of Palermo, Palermo, Italy
[3] Department of Physics and Astronomy, University of Florence, Florence, Italy
[4] European Laboratory for Non-Linear Spectroscopy, Florence, Italy
[5] National Institute of Optics, National Research Council (INO-CNR), Sesto Fiorentino, Italy
[6] Department of Neuroscience, Baylor College of Medicine, Houston, Texas, United States of America
[7] Institute of Nanoscience and Nanotechnology (IN2UB), University of Barcelona, Barcelona, Spain
[*] Authors to whom any correspondence should be addressed.

E-mail: pietro.ricci@ub.edu and giuseppe.santacaldo@unipa.it

Keywords: acousto-optics, neuroscience, imaging, optogenetics, AOD

Abstract

Cutting-edge methodologies and techniques are required to understand complex neuronal dynamics and pathological mechanisms. Among them, optical tools stand out due to their combination of non-invasiveness, speed, and precision. Examples include optical microscopy, capable of characterizing extended neuronal populations in small vertebrates at high spatiotemporal resolution, or all-optical electrophysiology and optogenetics, suitable for direct control of neuronal activity. However, these approaches necessitate progressively higher levels of accuracy, efficiency, and flexibility of illumination for observing fast entangled neuronal events at a millisecond time-scale over large brain regions. A promising solution is the use of acousto-optic deflectors (AODs). Based on exploiting the acousto-optic effects, AODs are high-performance devices that enable rapid and precise light deflection, up to MHz rates. Such high-speed control of light enables unique features, including random-access scanning or parallelized multi-beam illumination. Here, we survey the main applications of AODs in neuroscience, from fluorescence imaging to optogenetics. We also review the theory and physical mechanisms of these devices and describe the main configurations developed to accomplish flexible illumination strategies for a better understanding of brain function.

1. Introduction

A central quest in neuroscience is to unveil complex neuronal dynamics and understand their correlation to pathological conditions in vertebrate organisms [1–6] to clarify equivalent human neural mechanisms [7, 8]. In this framework, advanced light microscopy represents the tool of choice [9, 10] to non-invasively image extended neuronal populations [11, 12] at both cellular and subcellular scales [13]. This approach, in combination with genetically encoded calcium indicators, as reporters of neuronal activity [14, 15] (such as GCaMP [16]), paved the way for important progress in neuroscience, including high-resolution anatomical reconstruction [17], monitoring of biological sample development [18, 19], and advanced functional analysis [20, 21]. Furthermore, recent significant advancements in molecular biology have unlocked the potential for selectively altering the activity of neurons in the brain by means of light [22]. This breakthrough technique, known as optogenetics, has revolutionized the field of neuroscience [23] by enabling researchers to precisely control neural activity with unprecedented accuracy [24, 25]. To do this, optogenetic actuators, i.e. specific proteins, that work as light-gated ion channels [26], are expressed in genetically modified neurons. This makes these neurons photo-responsive such that they can be activated and inhibited by an external light trigger [27]. This remarkable technology not only offers a powerful tool for investigating the

complex functions of the brain, but it also has the potential to transform our understanding of neurological disorders, with the goal of supporting new therapeutic interventions [28]. As such, the development of optogenetics has been hailed as a revolution in experimental neuroscience and has opened exciting new paths for exploring the brain's inner workings.

However, imaging and optogenetics demand advanced tools to achieve more precise and efficient light delivery to specific regions of the brain and to obtain the possibility of analyzing fast and entangled neuronal events. In particular, optical microscopists strive for the best trade-off between precision, speed, and flexibility of targeted illumination [29, 30]. All these features are indeed necessary to selectively image specific groups of neurons and to control vast circuits in large brain volumes at millisecond time-scale, the typical dynamics of neuronal signalling. Wide-field illumination e.g. the most straightforward way to illuminate the sample, lacks spatial selectivity, making conventional microscopes unable to generate high-contrast or high-resolution images of thick samples. Point-scanning illumination, on the other hand, can obtain high-quality images with laser scanning confocal or multi-photon microscopy [31] but this approach is usually too slow to image the entire brain. This is a common issue with most point scanning procedures where a light beam needs to pivot throughout the whole field-of-view (FOV) for a complete reconstruction. Mechanical constraints, low illumination efficiency, and slow scanning speed limit the applicability of such devices in both imaging and optogenetics. For instance, galvanometer mirrors (GMs), due to their mechanical inertia, are rarely used in photostimulation but commonly in 2D raster scans [32, 33]. With their slow sweeping rate, they are not suitable for rapidly accessing connected neurons spread over large volumes. Making use of resonant GMs to increase the temporal resolution of such scanners up to frame rates of a few kHz is a possible solution for fluorescent imaging, but not for delivering custom stimulation patterns, as they do not provide the necessary flexibility for arbitrary excitation trajectories.

To deal with this issue, researchers developed more advanced scanners that enable the flexibility of addressing multiple target cells without losing spatiotemporal information [34]. To address preselected target regions simultaneously, illumination had to be parallelized. Particularly, several systems adopted micro-LEDs [35–37], digital micromirror devices (DMDs) [38, 39], or liquid crystal displays (LCDs) [40] for parallel and tailored illumination. However, even with refresh rates of up to tens of kHz, these systems suffer from poor stimulation efficiency in terms of laser power delivery when targeting far-spread targets. A more efficient parallel illumination approach has been achieved with computer-generated holography, which takes advantage of liquid-crystal-based spatial light modulators (LC-SLMs) [41–43]. However, such devices are not exempt from drawbacks. Speckle patterns are inherently generated at the sample plane by the repeated modulation of the wavefront phase, which has an impact on the precision of point illumination. In addition, cross-talk of the inter-pixel driving voltage limits the smallest available pixel size to $\sim 3\ \mu$m [44] which affects high-resolution illumination patterns. Therefore, only a few models provide the high refresh rate needed for advanced optogenetic stimulation (kHz). Indeed, even with continuous optogenetic stimulation, they are limited by the single actuator duty cycle ($10 \div 100$ ms), which does not match the fast ion-channel opening dynamics of many optogenetic actuators ($1 \div 2$ ms) [45]. Thus, successful studies concerning the activation dynamics of neuronal circuits that require faster illumination of multiple spots are not supported.

A promising step in this direction is the use of technologies that exploit the acousto-optic effect. In these cases, the interaction between ultrasound waves and light enables unprecedented control of light at microsecond time-scales [46]. For instance, tunable acoustic gradient index of refraction lenses (or TAG lenses) are today employed as varifocal lenses in remote focussing systems [47–51], acousto-optic tunable filters are often implemented as electronically adjustable narrow-band-pass filters [52–54], and acousto-optic modulators (AOMs) are used for a fast modulation of the diffracted beam intensity [55]. Arguably, though, the acousto-optic method that holds the greatest potential in neuroscience involves acousto-optic deflectors (AODs). First, these devices can rapidly deflect a light beam, control its intensity, and even its focusing without any mechanical movement. This allows AODs to attain MHz-order dynamics and meet the temporal requirements for concurrent activation of spatially distributed neurons. Second, the AOD response time for deflecting the light is constant, independent of the distance between successive targets. Thus, AODs guarantee excellent accuracy and consistency in beam positioning, offering high flexibility in targeting non-sequential areas of interest, better known as random-access scanning. Finally, it is also feasible to achieve the simultaneity promised by parallel approaches, creating several independent beams with a single device. This is possible by driving a single AOD simultaneously with multiple acoustic signals.

As shown in table 1, AODs stand out as the faster and more flexible option to target different regions in a volume, compared with the other aforementioned deflectors. Thanks to their versatility, AODs are increasingly exploited in experimental neuroscience, and we dedicate this review to collecting the most representative results achieved. Here, we first outline in detail the theory of AODs' physical functioning. Then, we explore the main configurations developed to accomplish flexible illumination strategies in various optical systems. Next, we discuss imaging and optogenetic applications realized with AODs. We also illustrate

Table 1. Comparison of typical illumination strategy, dwell time, and cost of implementation between different devices.

	GM	Res. GM	DMD	Micro-LED	LC-SLM	AOD
Illumination strategies	Sequential	Sequential	Parallel	Parallel	Parallel	Sequential Random-access Parallel
Dwell time/Refresh rate	0.5 ÷ 1 ms	100 μs	50 ÷ 200 μs	3 ÷ 100 ms	0.6 ÷ 10 ms	5 ÷ 30 μs
Cost	1 ÷ 3 k€	1 ÷ 10 k€	100 ÷ 1000 €	1 ÷ 5 k€	15 ÷ 20 k€	5 ÷ 10 k€

what can be achieved by driving a single AOD with multiple frequencies to parallelize the illumination. Finally, we discuss the possible drawbacks of these devices and solutions adopted to face them.

2. Operating theory and main implementations

The AODs' basic mechanism of light deflection resides in a periodic modulation of the refractive index of their acoustic-optic medium, which typically is a crystal of high refractive index, e.g. tellurium dioxide, TeO_2. This modulation is induced by a piezo-transducer directly bonded to the crystal and driven by an electrical signal at radio frequencies (30–350 MHz). The oscillating piezo generates a pressure wave—or sound wave—that propagates inside the medium and alters its optical properties. The induced periodicity of the refractive index defines a Bragg diffraction grating [56, 57], and a monochromatic impinging laser beam will be deflected at the first-order beam angle:

$$\theta_{\mathrm{d}} = \frac{\lambda}{\Lambda} = \frac{\lambda f}{\nu} \tag{1}$$

where λ and Λ are the light and sound wavelengths, respectively; f is the frequency of the driving signal; and ν is the soundwave propagation velocity in the medium, typically $\nu = 650$ m s^{-1} in TeO_2. A residual undiffracted beam, or zero-order beam 0th, will instead travel straight, carrying a small fraction of the incident optical power. Figure 1(a) shows schematically the beam diffraction by an AOD.

In any dynamic beam deflector, the two most important parameters are resolution and positioning speed. The maximum number of resolvable and distinct beam angles achievable by AOD light diffraction is given by the ratio of the angular deflector bandwidth $\Delta\theta$ and the angular divergence of the diffracted beam $\Delta\Phi$ [58]:

$$N = \frac{\Delta\theta}{\Delta\phi} \tag{2}$$

where $\Delta\Phi = \varepsilon\lambda/D$, with D being the incident beam's width and ε a nearly unitary factor that depends on the amplitude distribution of the incident beam (e.g. $\varepsilon = 4/\pi$ for a Gaussian beam). From equations (1) and (2) it follows that:

$$N \approx \Delta f \frac{D}{\nu} \tag{3}$$

where Δf is the frequency bandwidth of the AOD, i.e. the admitted range of acoustic frequency. It is noteworthy to mention that for non-monochromatic lasers, such as ultrafast pulsed lasers, the effect of spatial dispersion is to increase the angular spread of the beam as:

$$\Delta\theta_{\mathrm{dispersion}} = \frac{\Delta\lambda}{\Lambda} = \frac{\Delta\lambda f}{\nu}. \tag{4}$$

This means that whenever the spatial dispersion of the beam is significantly greater than the beam divergence $\Delta\Phi$, the maximum number of resolvable points N is accordingly reduced [59].

The ratio between the beam diameter and the soundwave propagation velocity in the medium defines a notable quantity, the access time:

$$T_a = \frac{D}{\nu}. \tag{5}$$

This is the necessary time for the acoustic wave to travel through the diameter of the laser beam. In other words, it is the time required for the beam to commute from one position to another, leading to an upper boundary on the AOD speed. Therefore, the parameter expressed in equation (3) is also known as the time-bandwidth product for an AOD.

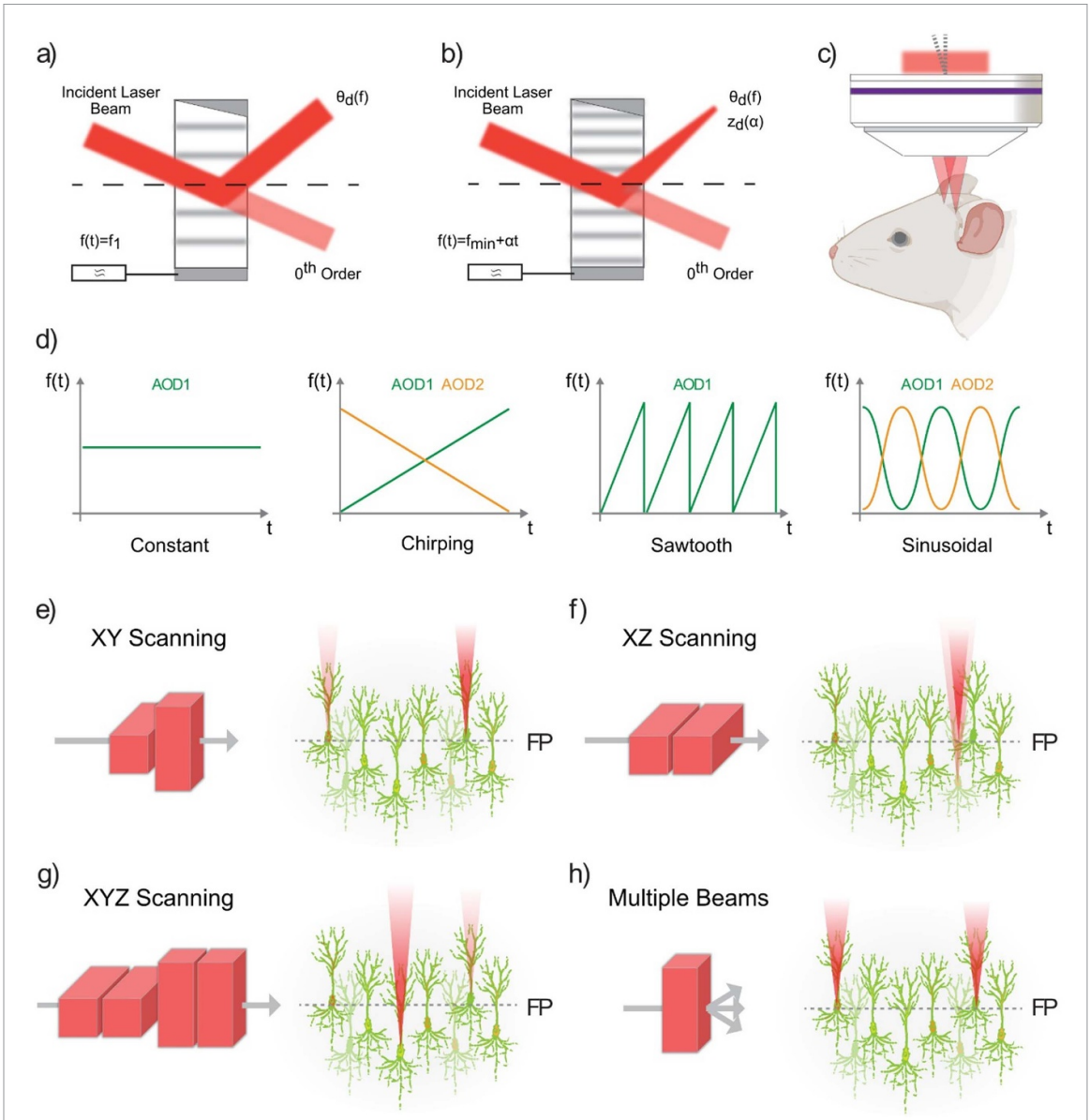

Figure 1. AOD illumination strategies. (a) AOD driven with single static frequency diffracts the incident laser beam at a frequency-dependent angle θ_d (f). 0th order is the residual un-diffracted beam. (b) AOD driven with time-varying frequency diffracts the laser beam both laterally and axially with frequency-dependent displacement. (c) Schematic of AO deflected laser beam projected on the sample through the illumination objective. (d) Main frequency profiles used to drive the AODs. (e)–(g) Default configuration of AODs used for lateral scanning in 2D (XY), axial scanning in 2D (XZ) and 3D scanning (XYZ), respectively. Relay optics between deflectors omitted. (h) An AOD simultaneously driven by multiple acoustic frequencies diffracts the input beam at corresponding angles, parallelizing the illumination. FP: focal plane.

Until now, we have only considered driving the piezo of these devices with a single and constant frequency (figure 1(d), first panel). However, the AOD's largest potential can be unlocked with several other driving configurations such as the one where an acoustic wave is characterized by a time-varying frequency. Figure 1(b) shows the schematic of AOD light diffraction with a chirped acoustic wave. Here, the angular deflection becomes a function of time [60, 61]:

$$\theta(x,t) = \frac{\lambda}{\nu} \cdot f\left(t + \frac{x}{\nu}\right) \tag{6}$$

where x indicates each point in the AOD's aperture with $x = 0$ being the laser spot centre. Then, a time-chirped acoustic frequency can be described as a function of its profile slope, or chirp α:

$$f(t) = f_{\min} + \alpha t \tag{7}$$

$$\alpha = \frac{(f_{\max} - f_{\min})}{T_{\text{scan}}} = \frac{\Delta f}{T_{\text{scan}}} \tag{8}$$

where T_{scan} is the time required to change the frequency from the minimum value f_{min} to the maximum f_{max}. Substituting this frequency expression in equation (6) we find:

$$\theta(x,t) = \frac{\lambda}{\nu} \cdot \left(f_{\text{min}} + \alpha t + \frac{\alpha x}{\nu}\right) = \frac{\lambda}{\nu} \cdot (f_{\text{min}} + \alpha t) + \frac{\lambda \alpha}{\nu^2} x. \tag{9}$$

This equation describes a convergent cylindrical lens, or acousto-optic lens (AOL), where the first term indicates an off-set central propagation axis that varies with time, i.e. called lateral drift. The inverse of the second term is the chirp-dependent focal length:

$$F_{\text{AOD}} = \frac{\nu^2}{\lambda \alpha}. \tag{10}$$

In other words, in a determined focal position, the beam moves laterally while the acoustic frequency is chirping. It is possible to compensate for this unwanted lateral drift by optically coupling the first AOD to a second one, driven with an opposite chirp (figure 1(d), second panel):

$$f_2(t) = f_{\text{max}} - \alpha t. \tag{11}$$

Synchronizing the two AODs, the light beam will impinge on two subsequent devices driven by counterpropagating sound waves travelling through their crystal. The total angular deviation that affects the beam, in this case, is:

$$\theta(x,t) = \frac{\lambda}{\nu} \cdot \left[f_1\left(t + \frac{x}{\nu}\right) + f_2\left(t - \frac{x}{\nu}\right)\right] = \frac{2\lambda f_C}{\nu} + \frac{2\lambda\alpha}{\nu^2} x \tag{12}$$

$$f_C = \frac{f_{\text{max}} + f_{\text{min}}}{2}. \tag{13}$$

The cylindrical lens described in equation (12) has a central propagation axis determined by the median driving frequency and a variable focal length that depends on the chirp. This configuration forms an active AOL capable of 3D scanning. Figure 1(c) shows a schematic of light beam projection on the sample through the illumination objective after AOL deflection. Moreover, when these devices are configured for volumetric targeting, to keep the spot at fixed coordinates for a longer time than T_{scan} it will be essential to regularly repeat the frequency scan with equal slopes, such as a sawtooth profile (figure 1(d), third panel). This is necessary as the acoustic bandwidth and thus T_{scan} is limited. In addition, several other frequency profiles can be used to modulate the acoustic wave propagating in the AODs. For example, it is possible to obtain a fast axial periodic scan with two AODs, by modulating the two counterpropagating waves with sinusoidal profiles [62] (figure 1(d), fourth panel).

Notably, it should be mentioned that acoustic frequency sweeping also makes the AOD resolution a dynamic quantity, reducing it compared to the static case:

$$N_{\text{d}} = N\left(1 - \frac{T_a}{T_{\text{scan}}}\right) + 1. \tag{14}$$

This means that the number of neuronal targets addressable by AOD-based systems depends on the acoustic wave frequency profile selected.

To summarize, AODs can be driven in different ways to freely deflect the light and project the beam on the sample. Using two AODs oriented orthogonally to each other, eventually optically conjugated via a 4-f telescope, provides a straightforward and fast way to control the beam in 2D, for example, for a planar raster scan (x-y scanning, figure 1(e)). Moreover, with two optically conjugated AODs oriented parallelly it is also possible to independently control the lateral deflection of the beam along one direction and its axial address (x-z scanning, figure 1(f)). To extend the light manipulation to a more general 3D scanning (x-y-z scanning, figure 1(g)), two more AODs are required to be implemented, for a total of four optically coupled devices. That is because, for each direction, it is necessary to compensate for the corresponding lateral drift discussed above.

Being intrinsically unaffected by inertia or any other mechanical constraints, these mentioned driving configurations provide an absolutely stable and steady way to achieve fast point scanning. Moreover, unlike any other standard beam scanning principles, each not-adjacent coordinate can be reached with the same access time, thus allowing for true random-access scanning. However, a finite time is still required to move from one coordinate to another, that is the access time needed to allow the soundwave to interact with the whole beam diameter, (typical access time: 10–30 us, see equation (5)). Therefore, it is important to highlight a different solution adopted by [63]. Introducing a slightly different chirp in equation (11) for the

counterpropagating wave in the second AOD results in a partial compensation of the lateral drift. Overall, this generates a movement of the beam spot along a line throughout the specified dwell time. In other words, by selecting proper acoustic frequencies, it is possible to generate fast and continuous lateral scans, with certain drift speeds, in a particular z-plane.

Even though with this approach the lateral beam position drifts continuously, interruptions are still required to jump from one plane to another. In 2016, the same group [64] further developed the earlier method by introducing a novel relationship between the focal spot coordinates and the chirp parameters of the four AODs. Briefly, this is a generalization of what was previously stated concerning the use of acoustic frequencies characterised by non-linear chirps, that vary in time according to parabolic profiles. Partial drift compensation with these particular acoustic frequency profiles allowed to define continuous trajectories in 3D with arbitrary directions and predetermined speeds [53].

2.1. Multibeam diffraction with AODs

Until this point, we have only considered driving each AOD with a single acoustic frequency. Even though AOD represents the fastest device commercially available to deflect light (up to hundreds of KHz), it enables only sequential, or random-access, scanning when driven with a single frequency at the time. It means that in this configuration, concurrent illumination of different targets, or neurons, is never obtained, but they can only be addressed subsequently. However, there is no limitation on the number of radio frequencies applied concurrently to the piezo other than avoiding exceeding the maximum power. When the piezo is simultaneously driven by different frequencies, multiple sound waves propagate through the crystal. In consequence, the impinging beam will interact with a linear combination of these waves and be simultaneously diffracted by different gratings [65, 66]. This principle enables the use of an AOD to parallelize the illumination and simultaneously deflect the input light under different angles (figure 1(h)). While this comes at the cost of power reduction for each diffracted beam—a common shortcoming in each light parallelization approach—it can be compensated by simply increasing the input light. Several methods exist to generate multi-frequency signals, ranging from simply combining the outputs of different generators or programming a complex dynamic waveform through an arbitrary waveform generator.

3. Applications in experimental neuroscience

In this chapter, we retrace the main results achieved with AODs in experimental neuroscience. Herein, we followed the evolution of the different AODs implementations and configurations, explaining how their different features and targeting strategies were exploited by neuroscientists in the past years. In detail, we collect the results in three separate sections: the first regards the imaging applications; the second concerns the uses of AODs to improve the capabilities of well-established imaging methods, such as light-sheet fluorescence microscopy (LSFM); the third reviews all the successes obtained with AODs for photostimulation of neuronal samples and optogenetics.

3.1. Imaging of neuronal populations with AODs

The first interest in using AODs for neuroimaging was driven by their scan rate advantage over GM-based scanners. With the simplest implementation of a single AOD, notable performances were reached in raster scans beyond video rates, i.e. above 30 Hz, both with single-photon [57] and multi-photon excitation [67, 68]. Another notable property of AODs led to the development of single-photon random-access fluorescence microscopes, where the excitation beam can be freely and quickly repositioned within the FOV [69]. For instance, by using voltage-sensitive dyes and Ca^{2+} indicators to monitor functional neuronal activity, multiple sites were imaged in μm-sized processes of cultured hippocampal neurons with up to 200 000 samples per second and a repositioning time between 3–5 μs. After that, with the introduction of a dispersion compensation scheme for ultrafast laser pulses [59], natural steps forward were moved toward AOD-based random-access multi-photon (RAMP) microscopy [70, 71], extending the range of applications. Among them, many different 2D and 3D scanning methods have been developed to concurrently or sequentially explore different regions of interest (ROIs) with high temporal and spatial resolution for structural imaging and functional neuronal activity recording, both for *ex vivo* and *in vivo* preparations. Figure 2(a) shows as examples, seven different targeting strategies: point-by-point, ribbon, snake and multi-3D-line scanning, chessboard and multi-layer multi-frame sampling, and multi-cube volumetric scanning [64]. Remarkable neural functional and structural investigations have been realized with 2D RAMP microscopes based on two crossed AODs [70–81]. Multi-ROI scan rates of 1 kHz or beyond [72, 75] have been demonstrated to track calcium activation in different cultured neuron populations and imaging large FOVs up to 0,5 $\times$ 0,5 mm^2

[77]. Here, we report two examples of the structural and functional measurements presented in Iyer *et al* [71, 75] and Otsu *et al* [75] as typical examples of what is achievable with AOD-based 2D RAMP microscopes. Figure 2(b) displays the maximum intensity projection (MIP) of a CA1 pyramidal neuron, revealing many apical dendrites [63]. Recordings at 500 Hz of Ca^{2+} transients from single optical sections at selected sites are superimposed. Figure 2(c) shows the MIP of a Purkinje cell [75], obtained by a sequential raster scan of 40 optical sections spaced every 1 mm, while figure 2(d) illustrates a single-plane image of the apical dendrite and of a proximal oblique dendrite of a layer V pyramidal neuron. The red dots indicate the positions of optical calcium-activation recordings displayed in figure 2(e). The upper trace exhibits a depolarizing current step triggered by an early spike and a tonic discharge of additional spikes on top of a depolarized plateau, while the lower traces show fluorescence transients recorded along the dendrite.

Interestingly, with two crossed AOD RAMP configuration, multi-beam illumination has also been investigated to parallelize the sampling of different ROIs. In particular, D'Angelo *et al* recorded *in vitro* the electrical activity from clusters of Purkinje cells [83] and cardiomyocytes with voltage-sensitive dyes [79].

The first attempts at using AODs for axial scanning enabled imaging and fluorescence lifetime imaging of neurons in mouse hippocampal tissue in the volume [84]. In detail, two planes of 100 × 100 μm, axially displaced by 40 μm were subsequently illuminated adjusting the frequency profile of the radio-signal driving the AODs, without moving the objective. Introducing an ETL or a piezo-scanner at the objective improved on this aspect but compromised the volumetric scan rate to 20–30 Hz for functional *in vivo* Ca^{2+} recording in mouse neocortex [85] and to 6 Hz for capturing sensory-evoked activity of the entire neurons within the developing brain of tadpoles [86].

Nevertheless, the full potential of this technique was achieved by employing two optically conjugated pairs of crossed AODs in 4-f configuration, as a 3D AOL [4, 63, 64, 82, 87–89]. This configuration supports repositioning speeds ranging from 30 μs down to 10 μs [88], which is important for capturing fast spontaneous neuronal microcircuit activity in the mouse cortex, and access volumes up to 1 mm^3 [63]. The very high sampling speed of 3D RAMP has enabled *in vivo* functional imaging studies in behaving mice using Ca^{2+} indicators, even with motion compensation [4, 64, 88, 89]. Figure 2(f) shows a 3D rendering of *in vivo* AOL-based volumetric structural imaging of neuronal dendrites and spines in a 150 μm depth range, labelled with the fluorescent dye Alexa 594 [82]. Another representative example of 3D AOL-based RAMP imaging is presented in figure 2(g), which displays an *in vivo* dendritic segment of a selected GCaMP6f-labeled neuron in a behaving mouse [64] recorded with the 3D ribbon scanning method in a volume of 140 × 70 × 80 μm^3. Figure 2(h) shows the longitudinal (left) and transverse (right) raw fluorescence scans (in green) and the average Ca^{2+} responses during spontaneous activity (in colour) [64], acquired along the blue ribbon denoted in *g*) and corrected for motion artefacts.

Finally, it is noteworthy the AODs' driving solution recently adopted by Villette *et al* [90] and Akemann *et al* [91], where the frequency- and amplitude-modulation of the acoustic wave is synchronized with the pulsed laser clock. In such a way, the focus drift associated with chirped AO gratings is abolished, and only two AODs are needed to access the sample very rapidly in 3D [92]. In particular, they used the submillisecond temporal resolution provided by this approach to probe cortical and hippocampal neurons in awake-behaving mice expressing high-gain voltage indicators [90] at 15 kHz, and GCaMP6f [91] at 40 kHz, respectively.

3.2. AOD in synergy with imaging systems

Recently, AODs have been used to enhance the capabilities of well-established imaging techniques. For instance, Tsyboulski *et al* [93] presented an innovative frequency-multiplexing imaging strategy based on AODs. In particular, they demonstrated the ability to encode multiple excitation spots with specific modulation frequencies and discussed promising perspectives for very fast monitoring of multisite calcium signals in brain tissues. Furthermore, 1D AOD-based slit-scanning has been used in combination with micro-optical sectioning tomography to confocally image thick mouse brain samples [94]. Nevertheless, AODs have given their largest contribution to another foundational technique: the LSFM. In detail, AODs have been successfully used to generate a scanning light sheet that illuminates sample planes in the fastest way possible, up to 0.8 million frames per second [95]. Such speed enabled plane-by-plane volumetric structural and functional imaging of *ex vivo* tissues and even of entire *in vivo* animals, including Caenorhabditis elegans, at tens of Hertz volume rates. In addition, using a crossed configuration of 2 AODs in the excitation arm and an acoustic varifocal lens in the detection path has allowed the realization of a fast inertia-free volumetric LSFM [96]. In the same context, single AODs have been successfully exploited to pivot the illumination beam and remove striping artefacts from the collected neuronal functional images in zebrafish [97] and mice [98], a well-known problem in LSFM [99] caused by scattering and/or absorption of light incident upon the sample through uneven lateral illumination. Notably, in these experiments, enhancing angular diversity in the illumination direction through simultaneous multibeam and/or rapid

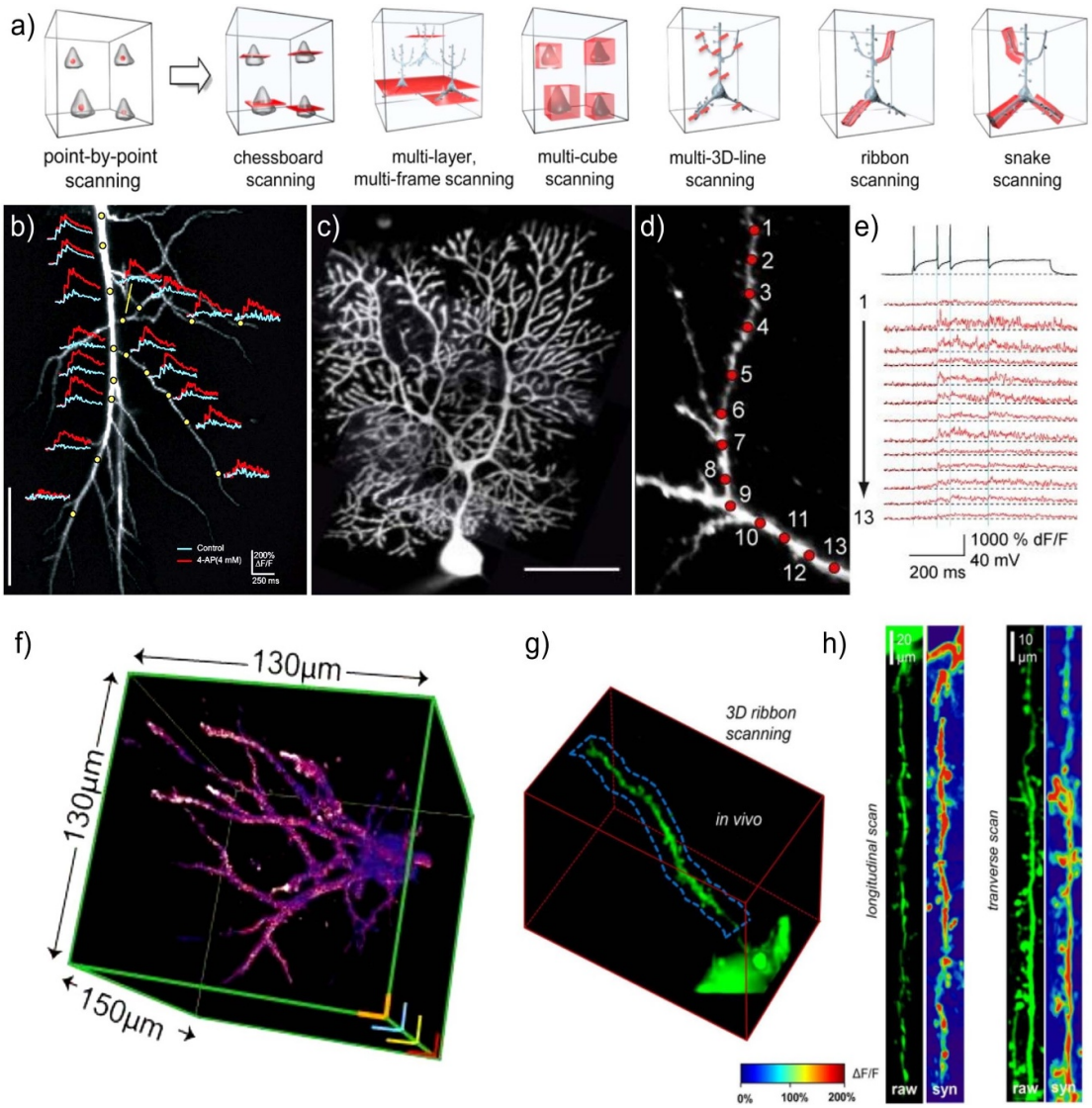

Figure 2. RAMP imaging applications of AODs. (a) Example of seven 3D scanning methods developed for *in vivo* imaging with motion compensation. The red points, lines, surfaces and volumes represent the addressed ROIs. Reproduced from [64]. CC BY 4.0. (b) MIP of a CA1 pyramidal neuron, revealing many apical dendrites. Recordings at 500 Hz of Ca^{2+} transients from a single optical section at selected sites are superimposed. Scale bar, 50 μm. Reproduced with permission from [71]. (c) MIP of a Purkinje cell, obtained by a sequential raster scan of 40 optical slices spaced every 1 μm. Scale bar: 50 μm. Reprinted from [75], Copyright (2008), with permission from Elsevier. (d) Single plane image of the apical dendrite and of a proximal oblique dendrite of a layer V pyramidal cell, the red dots indicate the positions of the optical recordings displayed in (e). Reprinted from [75], Copyright (2008), with permission from Elsevier. (e) Upper trace: a depolarizing current step triggered an early spike and a tonic discharge of additional spikes on top of a depolarized plateau. Lower traces: fluorescence transients recorded at the red dot positions in (d). Reprinted from [75], Copyright (2008), with permission from Elsevier. (f) 3D rendering of an AOL-based volumetric structural imaging of neuronal dendrites and spines over a 150 μm depth range, labelled with the fluorescent dye Alexa 594. Reprinted from [82], Copyright (2014), with permission from Elsevier. (g) 3D *in vivo* image of a dendritic segment of a selected GCaMP6f-labeled neuron in behaving mice recorded with the ribbon scanning method using 3D DRIFT AO. Red cube, $140 \times 70 \times 80$ μm^3. Reproduced from [64]. CC BY 4.0. (h) Longitudinal (left) and transverse (right) raw fluorescence scans (green) along the blue ribbon shown in (g), with motion artefacts elimination. Average Ca^{2+} responses along the ribbon during spontaneous activity (syn.) are colour-coded. Reproduced from [64]. CC BY 4.0.

scanning by AOD has demonstrated a reduction and even removal of striping. An example of such artefacts is shown in the upper panel of figure 3(a) where a sample of 15 μm polystyrene beads embedded in 1% agarose gel and immersed in water is imaged by illuminating with 1 (1LS) or 7 (7LS) static light sheets coming from different angles or with a single pivoted plane (SM). The green arrows indicate examples of striping artifacts almost suppressed in the 7LS and SM cases. The insets show the fluorescence intensity profiles along the y-axis, averaged over 6 μm around the white dotted line, clearly illustrating how the beads occlude the light-sheet propagation, affecting the image quality, and demonstrating that pivoted illumination significantly reduced striping artefacts. Figure 3(b) shows an *ex vivo* image of a cleared mouse brain expressing the fluorescent protein tdTomato where striping has been efficiently removed by exploiting such AOD beam pivoting in a confocal LSFM.

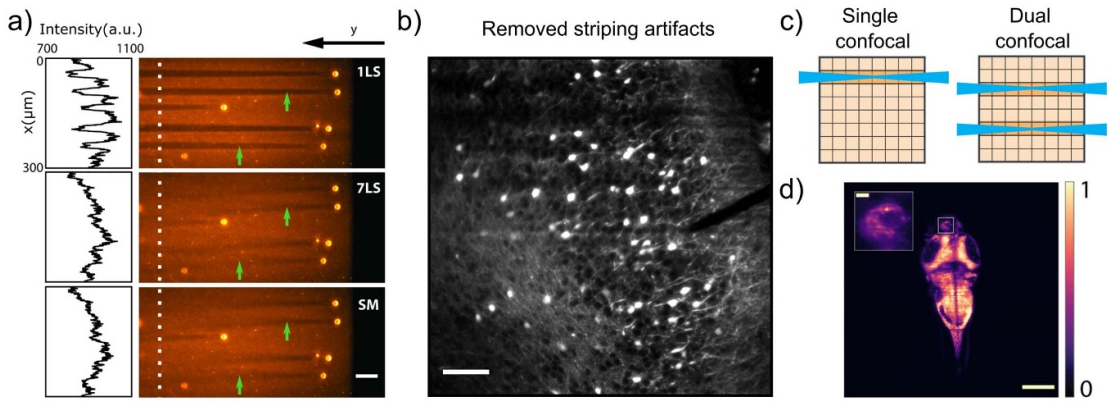

Figure 3. LSFM imaging applications of AODs. (a) LSFM images obtained with different AOD-generated light-sheet configurations (1 or 7 static light sheets at different angles and single-plane sweeping mode). The sample contains 15 μm polystyrene beads embedded in 1% agarose gel immersed in water. The insets show the fluorescence intensity profiles along the y-axis, averaged over 6 μm around the white dotted line. The line plots depict how the background becomes more uniform with an increasing number of illumination directions. The green arrows indicate the examples of striping artifacts in the three panels. White scale bar 50 μm. Reproduced from [97]. CC BY 4.0. (b) Confocal LSFM image of an area of a mouse brain expressing tdTomato, obtained by AOD-pivoted illumination of the sample. The image shows the effectiveness of the approach to remove striping artefacts from the images. Scale bar size: 100 μm. Reproduced with permission from [98]. (c) An AOD is used to generate simultaneously two light sheets that are concurrently imaged on a camera to double the acquisition speed of a confocal LSFM while preserving the properties of confocal detection. Reproduced from [100]CC BY 4.0. (d) Example image of zebrafish larva's neurons taken with the AOD-based dual LSFM, colour-coded in purple. The inset shows a 4x magnified left habenula area within the diencephalon where neural activity can be observed. Scale bar size: 200 μm; 20 μm in the inset. Reproduced from [100]. CC BY 4.0.

Moreover, the approach of driving the AODs concurrently with several radio-frequency signals has also been exploited to generate a stack of parallel light-sheets, enabling the simultaneous illumination of different sample planes and obtaining a fast volumetric image with high signal-to-noise ratio and contrast [101]. Finally, this method has been used to double the LFSM acquisition velocity by generating simultaneously two light sheets in combination with the advanced rolling shutter acquisition modes of a CMOS camera [100], as displayed in figure 3(c). Notably, this approach prevents any negative impact on the image quality, as demonstrated in figure 3(d) by imaging zebrafish larva's neuron nuclei with activity observable in the left habenula within the diencephalon (inset).

3.3. Targeted photostimulation and optogenetics with AODs

AODs can play a key role in direct optical stimulation as they enable precise light delivery to specific neurons or brain regions and the selective targeting of specific neural circuits in the brain. The main advantage of AODs is that they can position a laser beam within a volume with high temporal and spatial precision, making them ideal for optogenetic experiments. This means that researchers can activate or inhibit specific neurons with light pulses of varying duration, intensity, and location. However, while AODs have been widely used for imaging in experimental neuroscience, there have been relatively few reported applications of AOD-based optogenetic stimulation.

The first significant attempt to use AODs for photostimulation dates back to 2002 and demonstrated local and graded neuronal membrane currents following focal multisite UV illumination of a caged neurotransmitter [102]. In the following, Shoham *et al* [103] used AODs for rapidly and precisely controlling the release of neurotransmitters in specific locations of the brain. The researchers demonstrated that this technique can be used to selectively activate or inhibit the activity of neurons in the brain using UV light (355 nm) by single-photon excitation with both high temporal (20 000 locations per second) and spatial resolution. Figure 4(a) reports a two-photon image of a pyramidal neuron showing the selected sequential uncaging locations (numbers 1–10) on the apical dendrite and the related integration of electrical responses from the cell at different uncaging intervals.

After that, the next step was taken by Losavio *et al* [106] developing the first AOD-based two-photon microscope optimized for activating single neurons by their post-synaptic receptors using caged compounds. Contrary to single-photon excitation, the combination of two-photon excitation and AODs presented distinctive technical challenges. Ultrafast lasers, indeed, have a wider spectral content than continuous lasers, and since the AOD scanning principle relies on diffraction, compensation is necessary. The authors describe

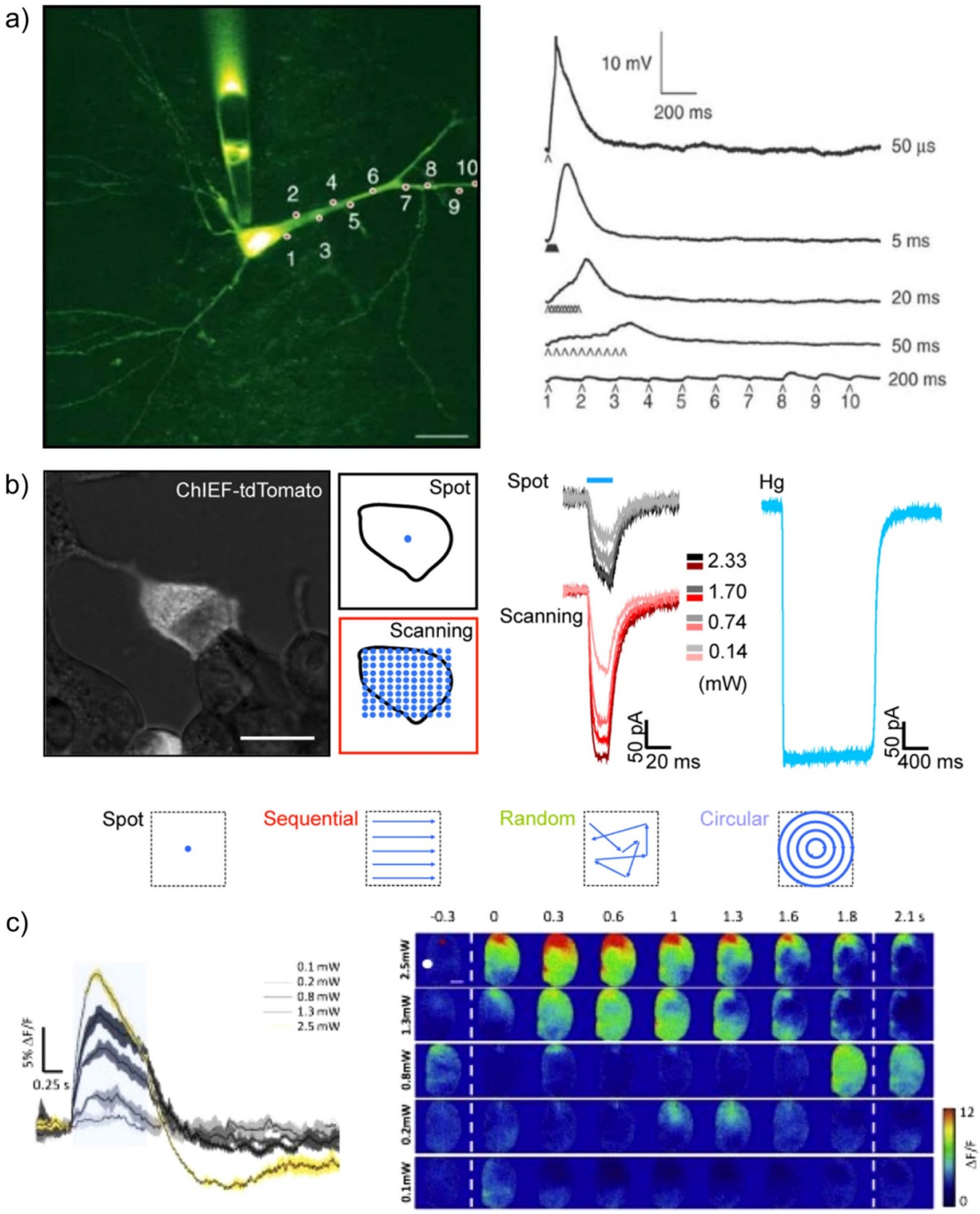

Figure 4. Applications of AODs for photostimulation and optogenetics. (a) Image and temporal traces of sequential photo-induced uncaging in different locations on an apical dendrite. Reproduced from [103], with permission from Springer Nature. (b) Optogenetic activation of HEK 293 cell expressing ChIEF-tdTomato and different activation patterns generated with AODs. Reproduced from [104] CC BY 3.0. (c) Calcium responses to the optogenetic stimulus train in mice cortex at different excitation power. Reproduced from [105]. CC BY 4.0.

a detailed and practical strategy to compensate for spectral and temporal dispersion, allowing for nearly diffraction-limited visualization of structures and the delivery of physiological stimuli.

A positive validation of using an AOD system for optical brain stimulation has been reported by direct activation of cell-expressing channelrhodopsins [104, 107, 108]. In these studies, the ability to selectively activate neurons using a single-photon [104, 107] and multiphoton [108] AOD-based system was demonstrated in cultured specimens (cells, neurons, and astrocytes) and the brains of mice, drosophila and zebrafish larvae. Figure 4(b) shows a HEK 293 cell expressing light-sensitive ChIEF-tdTomato together with the pattern of fixed-spot and whole-soma scanning photostimulation; membrane currents recorded in response to fixed-spot (dark) and whole-soma scanning (red) stimulations at different levels of laser power, together with such currents evoked by traditional Hg lamp illumination (cyan) is also shown. Four different

AOD-generated stimulation patterns show the large flexibility of the AOD scanning system that allows optimizing the excitation scheme for selectively covering the whole cell and scanning the laser across the cell in an ultra-fast manner (10–50 μs/site) [104].

Starting from there, AOD-based microscopy combined with genetically targeted expression of photoactive proteins has been used to highlight functional connections and synaptic plasticity in the mouse brain. Huang *et al* showed that learning tasks can affect the connectivity of interneurons in the olfactory bulb and that active learning can promote plasticity in connectivity maps [109]. Quast *et al* analyzed the development of inhibitory sensory maps and how they change over time, showing that inhibitory sensory maps become broader during development [110]. Hernandez *et al* discussed the use of optogenetics to induce complex patterns of activity in the cerebellar granular layer, showing that this technique can reveal insights into the integrative properties of this brain region [111].

A detailed analysis of the functional synaptic architecture of callosal inputs into the mouse's primary visual cortex has been reported by Lee *et al* [4]. The authors used optogenetic techniques to activate specific callosal inputs and found they could modulate the activity of both excitatory and inhibitory neurons in the cortex, showing that callosal inputs play an important role in shaping visual processing. Along the same lines, Conti *et al* analyzed functional connectivity in the brain using a large-scale double-path illumination system with a split FOV to enable the simultaneous measurement of inter- and intra-hemispheric functional connectivity [112]. AODs have been used in a combined rehabilitation approach for promoting the recovery of structural and functional features of healthy neuronal networks after stroke [113, 114]. Here, the authors used optogenetic techniques to selectively activate neurons in the cortex after stroke and found that a rehabilitation strategy based on combined physical and direct optogenetic stimulation of neural cells improves functional recovery and increases cortical activity. Furthermore, to probe specific neural activation features associated to relevant movements in awake mice, transcranial optogenetic stimulation by means of AODs, allowed to highlight the underlying neural connectivity [105]. Figure 4(c) shows representative average calcium responses to the optogenetic stimulus train at increasing laser powers in a mouse. The yellow line represents the calcium response threshold associated with complex movement execution. On the right, representative wide-field image sequences of cortical activation at different laser powers. The results suggest that this combined approach may be a promising therapeutic strategy for stroke recovery and to highlight cortex connectivity.

4. Discussion

As presented above, AODs respond to demands for light-addressing precision, high temporal resolution, random-access scanning, and multi-target illumination, making them appealing for a very wide variety of experiments. Table 2 summarizes several representative experimental results achieved in neuroimaging and optogenetics with AODs according to the specific configurations, light excitation modalities and characteristics.

Thanks to their high flexibility, these devices have been used to push the performance of different instruments designed for applications in experimental neuroscience. For instance, several light-sheet microscopes have benefited from the AODs' fast scanning rate.

However, despite their fundamental advantages, there is a drawback when AODs are used for axial focusing. This is because light transmission has an intrinsic dependency on the driving acoustic frequency. In particular, as a function of the chirp imposed on the driving frequency, the beam will spend different effective times illuminating spots in different planes, making the AODs in principle not well suited for uniform intensity axial photostimulation. To improve the power delivered within the pixel-to-pixel dwell time, the frequency ramps driving the AODs can be triggered repeatedly, effectively multiplying the minimum energy deposited on different focal planes [108]. Alternatively, to overcome this lack of uniformity in the axially released power distribution, it is possible to apply a pre-calibrated tuning of the driving signal amplitudes for each point addressed within the volume, flattening the distributions. With these approaches, we can expect an increased use of AODs in 3D optogenetic applications, which is lacking so far.

Moreover, 1P excitation strategies have been preferentially implemented with AOD-based microscopes. The use of AODs with femtosecond pulses raises, indeed, several technical difficulties. This is because ultrafast laser pulses needed for multiphoton illumination, experience significant spatial and temporal dispersion while propagating through AO materials. Recalling equation (1), the angle of deflection is wavelength-dependent and an ultrafast and thus wideband laser pulse is spatially dispersed by the AOD (equation (4)). At the same time, ultrafast lasers are affected by temporal dispersion when they propagate through dispersive materials, with a frequency-dependent index-of-refraction $n(\lambda)$. This is particularly evident for crystal materials commonly used in AOD, causing the temporal broadening of an ultrashort pulse. These effects of beam distortion and pulse broadening reduce the illumination efficiency, image

Table 2. Representative experimental results achieved in imaging and photostimulation of neuronal samples by using different AOD configurations, specimens, and parameters; 1PE and 2PE indicate one-photon and two-photon excitation of the sample, respectively; SHG: second harmonic generation.

Experimental purpose	Specimen	AOD configuration	Light excitation	Key parameters	Reference
Neuroimaging	Rat brain slice	2 AODs 2D Random-access	2PE	200 × 200 μm scanning area	[71]
	Rat brain slice	2 AODs 2D Random-access	2PE SHG	Simultaneous multisite recording	[83]
	Rat brain slice	4 AODs 3D Random-access	2PE	200 × 200 × 50 μm scanning volume	[85]
	Awake mice	4 AODs 3D Random-access	2PE	150 μm focal depth range	[82]
	Awake mice	4 AODs 3D Random-access	2PE	500 × 500 × 650 μm scanning volume	[64]
	Awake mice	2 AODs 3D Random-access	2PE	Serial sampling at 40 KHz	[91]
Photostimulation and Optogenetics	Rat brain slices	2 AODs 2D scanning	1PE	20 000 sites per second	[103]
	Cultured rat neurons	2 AODs	1PE	100 000 sites per second	[104]
	Drosophila brain	2D scanning			
	Mouse slices	2 AODs 2D scanning	1PE	>100 μm depth penetration	[111]
	Mice brain	4 AODs 3D Random-access	2PE	40% optogenetic activation	[4]
	Zebrafish larva brain	4 AODs 3D Random-access	2PE	75% optogenetic activation	[108]

resolution and signal-to-noise, making 2P excitation less attractive. Fortunately, several solutions have been proposed to face this issue. Iyer *et al* [59] developed a compact design introducing an additional diffraction grating after the AOD to strongly reduce the spatial dispersion, and a four-pass stacked-prism 'pre-chirper' for total compensation of the temporal dispersion. After that, it has been widely demonstrated [115, 116] how introducing a highly dispersive prism before the AOD(s), can simultaneously provide a large compensation of both temporal and spatial dispersion. Other alternatives rely on the implementation of a single AOM placed at 45° before the AODs [72], or of a special Keplerian telescope [117].

Notably, it has been demonstrated that AODs can be successfully applied *in vivo* experiments, where the sample animals are free to move. Even though light scanning over several targets usually assumes animal immobilization to avoid motion artefacts, this is not strictly required with AOD-based illumination. Indeed, artefacts and misleading results can be straightforwardly avoided by targeting each neuron with a tailored pattern of illumination covering the cell body [91] or by quickly drifting the excitation spot anticipating the displacement [64].

Furthermore, special attention must be paid when the AODs are used for multitarget illumination. The light power is not equally distributed among the different beams, as expected from an ordinary beam splitter. Each generated beam depletes the source beam approximately equally, but in this multifrequency condition, intermodulation orders can appear [65]. In fact, the light in each principal beam may be re-diffracted by another acousto-optic grating generated in the crystal at the same time. This produces a slight light-intensity cross-modulation and can generate unwanted beam deflections at frequencies defined by a combination of the main frequencies. However, it has been demonstrated [118] that the intermodulation beams can be strongly attenuated. They showed that when the acoustic oscillation period is shorter than the access time (see equation (5)), the distribution of light power of the diffracted beams can be considered proportional to the power distribution over the corresponding frequency components. A complementary approach is to generate generic multi-frequency driving signals for the AODs with highly attenuated intermodulation through an arbitrary waveform generator.

5. Conclusions

In this review, we provide the theory of AODs and a wide range of applications in experimental neuroscience where they have been successfully employed, significantly advancing the field. This technology represents a

viable alternative to other well-established light-addressing approaches developed in recent years. Indeed, the fast responsiveness, accuracy in light-targeting and random-access capability of AODs gradually made them a tool of choice for an increasing number of researchers utilizing optical approaches in neuroscience. In addition, the versatility and adaptability of AODs are continuously creating unexplored implementations and scenarios, such as 3D random-access optogenetics. In conclusion, we believe these devices will offer valuable possibilities to researchers, aiding in the study of increasingly complex neural systems, their disorders and pathologies, both *in-vivo* and *ex-vivo*.

Data availability statement

No new data were created or analysed in this study.

Acknowledgments

P R and M D received funding from the European Research Council (ERC) under the European Union's Horizon 2020 research and innovation program (Grant Agreement No. 101002460). M D is a Serra Hunter Professor. G S received funding from FFR 2023 of Unipa. V G has received funding from Next Generation EU, in the context of the National Recovery and Resilience Plan, M4C2 investment 1.2 [DD 247 19.08.2022] Project MicroSpinEnergy. This resource was financed also by the Next Generation EU [DD 247 19.08.2022]. F P received funding from the European Research Council (ERC) under the European program H2020 EXCELLENT SCIENCE (Grant Agreement No. 692943—BrainBIT and No. 966623—DAPTOMIC). The views and opinions expressed are only those of the authors and do not necessarily reflect those of the European Union or the European Commission. Neither the European Union nor the European Commission can be held responsible for them.

Conflict of interest

The authors declare no conflicts of interest.

ORCID iDs

Pietro Ricci https://orcid.org/0000-0002-6931-9234
Giuseppe Sancataldo https://orcid.org/0000-0002-8661-5895
Vladislav Gavryusev https://orcid.org/0000-0001-7734-7828
Francesco Saverio Pavone https://orcid.org/0000-0002-0675-3981
Peter Saggau https://orcid.org/0000-0002-6335-7475
Martí Duocastella https://orcid.org/0000-0003-4687-8233

References

[1] Adoff M D, Climer J R, Davoudi H, Marvin J S, Looger L L and Dombeck D A 2021 The functional organization of excitatory synaptic input to place cells *Nat. Commun.* **12** 1–15
[2] Turrini L *et al* 2017 Optical mapping of neuronal activity during seizures in zebrafish *Sci. Rep.* **7** 1–12
[3] Turrini L, Roschi L, de Vito G, Pavone F S and Vanzi F 2023 Imaging approaches to investigate pathophysiological mechanisms of brain disease in zebrafish *Int. J. Mol. Sci.* **24** 9833
[4] Lee K S, Vandemark K, Mezey D, Shultz N and Fitzpatrick D 2019 Functional synaptic architecture of callosal inputs in mouse primary visual cortex *Neuron* **101** 421–8.e5
[5] de Vito G *et al* 2022 Fast whole-brain imaging of seizures in zebrafish larvae by two-photon light-sheet microscopy *Biomed. Opt. Express* **13** 1516
[6] Adam Y 2021 All-optical electrophysiology in behaving animals *J. Neurosci. Methods* **353** 109101
[7] Bhattacharya M, Ghosh S, Malick R C, Patra B C and Das B K 2018 Therapeutic applications of zebrafish (Danio rerio) miRNAs linked with human diseases: a prospective review *Gene* **679** 202–11
[8] Santoriello C, Zon L I, Santoriello C and Zon L I 2012 Hooked! Modeling human disease in zebrafish *J. Clin. Invest.* **122** 2337–43
[9] Emiliani V, Cohen A E, Deisseroth K and Häusser M 2015 All-optical interrogation of neural circuits *J. Neurosci.* **35** 13917–26
[10] Werley C A, Brookings T, Upadhyay H, Williams L A, McManus O B and Dempsey G T 2017 All-optical electrophysiology for disease modeling and pharmacological characterization of neurons *Curr. Protocols Pharmacol.* **2017** 11.20.1–24
[11] Ji N, Freeman J and Smith S L 2016 Technologies for imaging neural activity in large volumes *Nat. Neurosci.* **19** 1154–64
[12] Ahrens M B, Orger M B, Robson D N, Li J M and Keller P J 2013 Whole-brain functional imaging at cellular resolution using light-sheet microscopy *Nat. Methods* **10** 413–20
[13] Vladimirov N *et al* 2018 Brain-wide circuit interrogation at the cellular level guided by online analysis of neuronal function *Nat. Methods* **15** 1117–25
[14] Dana H *et al* 2019 High-performance calcium sensors for imaging activity in neuronal populations and microcompartments *Nat. Methods* **16** 649–57
[15] Helassa N, Podor B, Fine A and Török K 2016 Design and mechanistic insight into ultrafast calcium indicators for monitoring intracellular calcium dynamics *Sci. Rep.* **6** 1–14

[16] Akerboom J *et al* 2012 Optimization of a GCaMP calcium indicator for neural activity imaging *J. Neurosci.* **32** 13819–40
[17] Denk W, Delaney K R, Gelperin A, Kleinfeld D, Strowbridge B W, Tank D W and Yuste R 1994 Anatomical and functional imaging of neurons using 2-photon laser scanning microscopy *J. Neurosci. Methods* **54** 151–62
[18] Keller P J, Schmidt A D, Wittbrodt J and Stelzer E H K 2008 Reconstruction of zebrafish early embryonic development by scanned light sheet microscopy *Science* **322** 1065–9
[19] Wan Y, McDole K and Keller P J 2019 Light-sheet microscopy and its potential for understanding developmental processes *Annu. Rev. Cell Dev. Biol.* **35** 655–81
[20] Wolf S, Supatto W, Debrégeas G, Mahou P, Kruglik S G, Sintes J M, Beaurepaire E and Candelier R 2015 Whole-brain functional imaging with two-photon light-sheet microscopy *Nat. Methods* **12** 379–80
[21] Lemon W C, Pulver S R, Höckendorf B, McDole K, Branson K, Freeman J and Keller P J 2015 Whole-central nervous system functional imaging in larval Drosophila *Nat. Commun.* **6** 7924
[22] Deisseroth K 2011 Optogenetics *Nat. Methods* **8** 26–29
[23] Yizhar O, Fenno L E, Davidson T J, Mogri M and Deisseroth K 2011 Optogenetics in neural systems *Neuron* **71** 9–34
[24] Papagiakoumou E 2013 Optical developments for optogenetics *Biol. Cell* **105** 443–64
[25] Emiliani V *et al* 2022 Optogenetics for light control of biological systems *Nat. Rev. Method Primers* **2** 1–50
[26] Lórenz-Fonfría V A and Heberle J 2014 Channelrhodopsin unchained: structure and mechanism of a light-gated cation channel *Biochim. Biophys. Acta (BBA)* **1837** 626–42
[27] Nagel G, Szellas T, Huhn W, Kateriya S, Adeishvili N, Berthold P, Ollig D, Hegemann P and Bamberg E 2003 Cation-selective membrane channel *Proc. Natl Acad. Sci.* **100** 13940–5
[28] Montagni E, Resta F, Mascaro A L A and Pavone F S 2019 Optogenetics in brain research: from a strategy to investigate physiological function to a therapeutic tool *Photonics* **6** 92
[29] Sancataldo G, Silvestri L, Letizia A, Mascaro A, Sacconi L and Pavone F S 2019 Advanced fluorescence microscopy for in vivo imaging of neuronal activity *Optica* **6** 758–65
[30] Ronzitti E, Ventalon C, Canepari M, Forget B C, Papagiakoumou E and Emiliani V 2017 Recent advances in patterned photostimulation for optogenetics *J. Opt.* **19** 113001
[31] Wang K, Horton N G and Xu C 2013 Going deep: brain imaging with multi-photon microscopy *Opt. Photonics News* **24** 32
[32] Wang H *et al* 2007 High-speed mapping of synaptic connectivity using photostimulation in Channelrhodopsin-2 transgenic mice *Proc. Natl Acad. Sci. USA* **104** 8143–8
[33] Petreanu L, Mao T, Sternson S M and Svoboda K 2009 The subcellular organization of neocortical excitatory connections *Nature* **457** 1142–5
[34] Ronzitti E, Emiliani V and Papagiakoumou E 2018 Methods for three-dimensional all-optical manipulation of neural circuits *Front. Cell Neurosci.* **12** 469
[35] Grossman N *et al* 2010 Multi-site optical excitation using ChR2 and micro-LED array *J. Neural Eng.* **7** 016004
[36] Yasunaga H, Takeuchi H, Mizuguchi K, Nishikawa A, Loesing A, Ishikawa M, Kamiyoshihara C, Setogawa S, Ohkawa N and Sekiguchi H 2022 MicroLED neural probe for effective in vivo optogenetic stimulation *Opt. Express* **30** 40292
[37] Peterson T, Mann S, Sun B L, Peng L, Cai H and Liang R 2023 Motionless volumetric structured light sheet microscopy *Biomed. Opt. Express* **14** 2209
[38] Wang S, Szobota S, Wang Y, Volgraf M, Liu Z, Sun C, Trauner D, Isacoff E Y and Zhang X 2007 All optical interface for parallel, remote, and spatiotemporal control of neuronal activity *Nano Lett.* **7** 3859–63
[39] Zhu P, Fajardo O, Shum J, Zhang Schärer Y P and Friedrich R W 2012 High-resolution optical control of spatiotemporal neuronal activity patterns in zebrafish using a digital micromirror device *Nat. Protocols* **7** 1410–25
[40] Stirman J N, Crane M M, Husson S J, Wabnig S, Schultheis C, Gottschalk A and Lu H 2011 Real-time multimodal optical control of neurons and muscles in freely behaving Caenorhabditis elegans *Nat. Methods* **8** 153–8
[41] Chaigneau E, Ronzitti E, Gajowa M A, Soler-Llavina G J, Tanese D, Brureau A Y B, Papagiakoumou E, Zeng H and Emiliani V 2016 Two-photon holographic stimulation of ReaChR *Front. Cell Neurosci.* **10** 234
[42] Nikolenko V, Watson B O, Araya R, Woodruff A, Peterka D S and Yuste R 2008 SLM microscopy: scanless two-photon imaging and photostimulation with spatial light modulators *Front. Neural Circuits* **2** 1–14
[43] Faini G *et al* 2023 Ultrafast light targeting for high-throughput precise control of neuronal networks *Nat. Commun.* **14** 1888
[44] Mansha S, Moitra P, Xu X, Mass T W W, Veetil R M, Liang X, Li S-Q, Paniagua-Domínguez R and Kuznetsov A I 2022 High resolution multispectral spatial light modulators based on tunable Fabry-Perot nanocavities *Light* **11** 141
[45] Lin J Y 2011 A user's guide to channelrhodopsin variants: features, limitations and future developments *Exp. Physiol.* **96** 19–25
[46] Duocastella M, Surdo S, Zunino A, Diaspro A and Saggau P 2021 Acousto-optic systems for advanced microscopy *J. Phys. Photonics* **3** 012004
[47] Kang S, Dotsenko E, Amrhein D, Arnold C B and Theriault C 2018 Ultra-high-speed variable focus optics for novel applications in advanced imaging *Proc. SPIE 10539, Photonic Instrumentation Engineering V* **1053902**
[48] Kang S, Duocastella M and Arnold C B 2020 Variable optical elements for fast focus control *Nat. Photon.* **14** 533–42
[49] Grulkowski I, Szulzycki K and Wojtkowski M 2014 Microscopic OCT imaging with focus extension by ultrahigh-speed acousto-optic tunable lens and stroboscopic illumination *Opt. Express* **22** 31746
[50] Yang X, Jiang B, Song X, Wei J and Luo Q 2017 Fast axial-scanning photoacoustic microscopy using tunable acoustic gradient lens *Opt. Express* **25** 7349
[51] Alexandropoulos C and Duocastella M 2023 Video-rate quantitative phase imaging with dynamic acousto-optic defocusing *Opt. Lasers Eng.* **169** 107692
[52] Windels F W, Pustovoit V I and Leroy O 2000 Collinear acousto-optic diffraction using two nearby sound frequencies *Ultrasonics* **38** 586–9
[53] Kutuza I B, Pozhar V E and Pustovoit V I 2003 AOTF-based imaging spectrometer for research of small-size biological objects *In: European Conf. on Biomedical Optics* pp 5143_165
[54] Pustovoit V I, Pozhar V E, Mazur M M, Shorin V N, Kutuza I B and Perchik A V 2005 Double-AOTF spectral imaging system *Proc. SPIE* **5953** 59530
[55] de Lima M M, Beck M, Hey R and Santos P V 2006 Compact Mach-Zehnder acousto-optic modulator *Appl. Phys. Lett.* **89** 121104
[56] Gottlieb M, Ireland C L and Ley J M 1983 *Electro-optic and Acousto-optic Scanning and Deflection* (MDI)
[57] Xu J and Stroud R 1992 *Acousto-optic Devices: Principles, Design, and Applications* (Wiley)
[58] Bass M 1994 *Handbook of Optics, Volume II—Devices, Measurements, and Properties* (Optical Society Of America, McGraw-Hill Education)

[59] Iyer V, Losavio B E and Saggau P 2003 Compensation of spatial and temporal dispersion for acousto-optic multiphoton laser-scanning microscopy *J. Biomed. Opt.* **8** 460
[60] Reddy G D and Saggau P 2005 Fast three-dimensional laser scanning scheme using acousto-optic deflectors *J. Biomed. Opt.* **10** 064038
[61] Reddy G D and Saggau P 2013 High-speed two-photon imaging *Cold Spring Harb. Protocols* **8** 1–7
[62] Kaplan A, Friedman N and Davidson N 2001 Acousto-optic lens with very fast focus scanning *Opt. Lett.* **26** 1078–80
[63] Katona G, Szalay G, Maák P, Kaszás A, Veress M, Hillier D, Chiovini B, Vizi E S, Roska B and Rózsa B 2012 Fast two-photon in vivo imaging with three-dimensional random-access scanning in large tissue volumes *Nat. Methods* **9** 201–8
[64] Szalay G *et al* 2016 Fast 3D imaging of spine, dendritic, and neuronal assemblies in behaving animals *Neuron* **92** 723–38
[65] Hecht D L 1977 Multifrequency acoustooptic diffraction *IEEE Trans. Sonics Ultrason.* **24** 7–18
[66] Antonov S N and Rezvov Y G 2007 Efficient multiple-beam Bragg acoustooptic diffraction with phase optimization of a multifrequency acoustic wave *Tech. Phys.* **52** 1053–60
[67] Lechleiter J D, Lin D T and Sieneart U 2002 Multi-photon laser scanning microscopy using an acoustic optical deflector *Biophys. J.* **83** 2292–9
[68] Roorda R D, Hohl T M, Toledo-Crow R and Miesenböck G 2004 Video-rate nonlinear microscopy of neuronal membrane dynamics with genetically encoded probes *J. Neurophysiol.* **92** 609–21
[69] Saggau P, Bullen A and Patel S S 1998 Acousto-optic random-access laser scanning microscopy: fundamentals and applications to optical recording of neuronal activity *Cell Mol. Biol.* **44** 827–46
[70] Iyer V, Hoogland T, Losavio B E, Fink R, Gaddi R, Patel S, Larson A and Saggau P 2005 Acousto-optic multiphoton laser scanning microscopy (AO-MPLSM) for structural and functional imaging in living brain slices *Proc. SPIE* **5700** 90–101
[71] Iyer V, Hoogland T M and Saggau P 2006 Fast functional imaging of single neurons using random-access multiphoton (RAMP) microscopy *J. Neurophysiol.* **95** 535–45
[72] Salomé R, Kremer Y, Dieudonné S, Léger J F, Krichevsky O, Wyart C, Chatenay D and Bourdieu L 2006 Ultrafast random-access scanning in two-photon microscopy using acousto-optic deflectors *J. Neurosci. Methods* **154** 161–74
[73] Lv X, Zhan C, Zeng S, Chen W R and Luo Q 2006 Construction of multiphoton laser scanning microscope based on dual-axis acousto-optic deflector *Rev. Sci. Instrum.* **77** 046101
[74] Diana M A, Otsu Y, Maton G, Collin T, Chat M and Dieudonné S 2007 T-type and L-type Ca^{2+} conductances define and encode the bimodal firing pattern of vestibulocerebellar unipolar brush cells *J. Neurosci.* **27** 3823
[75] Otsu Y, Bormuth V, Wong J, Mathieu B, Dugué G P, Feltz A and Dieudonné S 2008 Optical monitoring of neuronal activity at high frame rate with a digital random-access multiphoton (RAMP) microscope *J. Neurosci. Methods* **173** 259–70
[76] Grewe B F, Langer D, Kasper H, Kampa B M and Helmchen F 2010 High-speed in vivo calcium imaging reveals neuronal network activity with near-millisecond precision *Nat. Methods* **7** 399–405
[77] Jiang R, Zhou Z, Lv X and Zeng S 2012 Wide-band acousto-optic deflectors for large field of view two-photon microscope *Rev. Sci. Instrum.* **83** 043709
[78] Cesana E, Pietrajtis K, Bidoret C, Isope P, D'Angelo E, Dieudonné S and Forti L 2013 Granule cell ascending axon excitatory synapses onto golgi cells implement a potent feedback circuit in the cerebellar granular layer *J. Neurosci.* **33** 12430–46
[79] Sacconi L *et al* 2013 Probing cell activity in random access modality *Proc. SPIE* 880406 (available at: https://opg.optica.org/abstract.cfm?uri=ECBO-2013-880406)
[80] Otsu Y *et al* 2014 Activity-dependent gating of calcium spikes by A-type K+ channels controls climbing fiber signaling in purkinje cell dendrites *Neuron* **84** 137–51
[81] Shao Y, Qin W, Liu H, Qu J, Peng X, Niu H and Gao B Z 2012 Ultrafast, large-field multiphoton microscopy based on an acousto-optic deflector and a spatial light modulator *Opt. Lett.* **37** 2532
[82] Fernández-Alfonso T, Nadella K M N S, Iacaruso M F, Pichler B, Roš H, Kirkby P A and Silver R A 2014 Monitoring synaptic and neuronal activity in 3D with synthetic and genetic indicators using a compact acousto-optic lens two-photon microscope *J. Neurosci. Methods* **222** 69–81
[83] D'Angelo E, Sacconi L, O'Connor R P, Pavone F S, Mapelli J, Gandolfi D and Lotti J 2008 Optical recording of electrical activity in intact neuronal networks with random access second-harmonic generation microscopy *Opt. Express* **16** 14910–21
[84] Vučinić D and Sejnowski T J 2007 A compact multiphoton 3D imaging system for recording fast neuronal activity *PLoS One* **2** e699
[85] Grewe B F, Voigt F F, van't Hoff M and Helmchen F 2011 Fast two-layer two-photon imaging of neuronal cell populations using an electrically tunable lens *Biomed. Opt. Express* **2** 2035
[86] Sakaki K D R, Podgorski K, Dellazizzo Toth T A, Coleman P and Haas K 2020 Comprehensive imaging of sensory-evoked activity of entire neurons within the awake developing brain using ultrafast AOD-based random-access two-photon microscopy *Front. Neural Circuits* **14** 1–18
[87] Duemani Reddy G, Kelleher K, Fink R and Saggau P 2008 Three-dimensional random access multiphoton microscopy for functional imaging of neuronal activity *Nat. Neurosci.* **11** 713–20
[88] Cotton R J, Froudarakis E, Storer P, Saggau P and Tolias A S 2013 Three-dimensional mapping of microcircuit correlation structure *Front. Neural Circuits* **7** 1–13
[89] Nadella K M N S, Roš H, Baragli C, Griffiths V A, Konstantinou G, Koimtzis T, Evans G J, Kirkby P A and Silver R A 2016 Random-access scanning microscopy for 3D imaging in awake behaving animals *Nat. Methods* **13** 1001–4
[90] Villette V *et al* 2019 Ultrafast two-photon imaging of a high-gain voltage indicator in awake behaving mice *Cell* **179** 1590–608.e23
[91] Akemann W, Wolf S, Villette V, Mathieu B, Tangara A, Fodor J, Ventalon C, Léger J F, Dieudonné S and Bourdieu L 2022 Fast optical recording of neuronal activity by three-dimensional custom-access serial holography *Nat. Methods* **19** 100–10
[92] Akemann W, Léger J-F, Ventalon C, Mathieu B, Dieudonné S and Bourdieu L 2015 Fast spatial beam shaping by acousto-optic diffraction for 3D non-linear microscopy *Opt. Express* **23** 28191
[93] Tsyboulski D, Orlova N and Saggau P 2017 Amplitude modulation of femtosecond laser pulses in the megahertz range for frequency-multiplexed two-photon imaging *Opt. Express* **25** 9435
[94] Qi X, Yang T, Li L, Wang J, Zeng S and Lv X 2015 Fluorescence micro-optical sectioning tomography using acousto-optical deflector-based confocal scheme *Neurophotonics* **2** 041406
[95] Martin C, Li T, Hegarty E, Zhao P, Mondal S and Ben-Yakar A 2018 Line excitation array detection fluorescence microscopy at 0.8 million frames per second *Nat. Commun.* **9** 1–10
[96] Duocastella M, Sancataldo G, Saggau P, Ramoino P, Bianchini P and Diaspro A 2017 Fast inertia-free volumetric light-sheet microscope *ACS Photonics* **4** 1797–804

[97] Sancataldo G, Gavryusev V, de Vito G, Turrini L, Locatelli M, Fornetto C, Tiso N, Vanzi F, Silvestri L and Pavone F S 2019 Flexible multi-beam light-sheet fluorescence microscope for live imaging without striping artifacts *Front. Neuroanat.* **13** 1–8
[98] Ricci P, Sancataldo G, Gavryusev V, Franceschini A, Müllenbroich M C, Silvestri L and Pavone F S 2020 Fast multi-directional DSLM for confocal detection without striping artifacts *Biomed. Opt. Express* **11** 3111
[99] Ricci P, Gavryusev V, Müllenbroich C, Turrini L, de Vito G, Silvestri L, Sancataldo G and Pavone F S 2022 Removing striping artifacts in light-sheet fluorescence microscopy: a review *Prog. Biophys. Mol. Biol.* **168** 52–65
[100] Gavryusev V *et al* 2019 Dual-beam confocal light-sheet microscopy via flexible acousto-optic deflector *J. Biomed. Opt.* **24** 1
[101] Zunino A, Garzella F, Trianni A, Saggau P, Bianchini P, Diaspro A and Duocastella M 2021 Multiplane encoded light-sheet microscopy for enhanced 3D imaging *ACS Photonics* **8** 3385–93
[102] Iyer V, Losavio B E, Patel S S and Saggau P Ultraviolet acousto-optic laser scanner for fast, graded, multi-site photolysis of caged neurotransmitter to investigate dendritic integration *Proc. 2nd Joint 24th Annual Conf. and the Annual Fall Meeting Biomedical Engineering Society] [Engineering in Medicine and Biology]* (*Houston, TX, USA, 2002*) vol 3 (IEEE) pp 2101–2
[103] Shoham S, O'Connor D H, Sarkisov D V and Wang S S H 2005 Rapid neurotransmitter uncaging in spatially defined patterns *Nat. Methods* **2** 837–43
[104] Wang K, Liu Y, Li Y, Guo Y, Song P, Zhang X, Zeng S and Wang Z 2011 Precise spatiotemporal control of optogenetic activation using an acousto-optic device *PLoS One* **6** e28468
[105] Resta F, Montagni E, de Vito G, Scaglione A, Allegra Mascaro A L and Pavone F S 2022 Large-scale all-optical dissection of motor cortex connectivity shows a segregated organization of mouse forelimb representations *Cell Rep.* **41** 111627
[106] Losavio B E, Iyer V and Saggau P 2009 Two-photon microscope for multisite microphotolysis of caged neurotransmitters in acute brain slices *J. Biomed. Opt.* **14** 064033
[107] Liu Y, Zhao Y, Lv X, Li Y, Zhang X, Zhang J, Wang L and Zeng S 2012 Instrumentation of a compact random-access photostimulator based on acousto-optic deflectors *Rev. Sci. Instrum.* **83** 025116
[108] Ricci P *et al* 2022 Power-effective scanning with AODs for 3D optogenetic applications *J. Biophotonics* **15** e202100256
[109] Huang L, Ung K, Garcia I, Quast K B, Cordiner K, Saggau P and Arenkiel B R 2016 Task learning promotes plasticity of interneuron connectivity maps in the olfactory bulb *J. Neurosci.* **36** 8856–71
[110] Quast K B *et al* 2017 Developmental broadening of inhibitory sensory maps *Nat. Neurosci.* **20** 189–99
[111] Hernandez O, Pietrajtis K, Mathieu B and Dieudonné S 2018 Optogenetic stimulation of complex spatio-temporal activity patterns by acousto-optic light steering probes cerebellar granular layer integrative properties *Sci. Rep.* **8** 1–16
[112] Conti E, Mascaro A L A and Pavone F S 2019 Large scale double-path illumination system with split field of view for the all-optical study of inter-and intra-hemispheric functional connectivity on mice *Methods Protocols* **2** 1–11
[113] Allegra Mascaro A L *et al* 2019 Combined rehabilitation promotes the recovery of structural and functional features of healthy neuronal networks after stroke *Cell Rep.* **28** 3474–85.e6
[114] Conti E, Scaglione A, de Vito G, Calugi F, Pasquini M, Pizzorusso T, Micera S, Allegra Mascaro A L and Pavone F S 2022 Combining optogenetic stimulation and motor training improves functional recovery and perilesional cortical activity *Neurorehabil. Neural Repair* **36** 107–18
[115] Bi K, Zeng S, Xue S, Sun J, Lv X, Li D and Luo Q 2006 Position of the prism in a dispersion-compensated acousto-optic deflector for multiphoton imaging *Appl. Opt.* **45** 8560–5
[116] Zeng S, Lv X, Bi K, Zhan C, Li D, Chen W R, Xiong W, Jacques S L and Luo Q 2007 Analysis of the dispersion compensation of acousto-optic deflectors used for multiphoton imaging *J. Biomed. Opt.* **12** 024015
[117] Hu Q, Zhou Z, Lv X and Zeng S 2016 Compensation of spatial dispersion of an acousto-optic deflector with a special Keplerian telescope *Opt. Lett.* **41** 207
[118] Antonov S N 2005 Angular splitting of the bragg diffraction order in an acoustooptical modulator due to a frequency-modulated acoustic wave *Tech. Phys.* **50** 513–6